01/07/2024 07:42

(Article begins on next page)

IMPREGNATED CARBON FABRIC REINFORCED CEMENTITIOUS MATRIX COMPOSITE FOR REHABILITATION OF THE FINALE EMILIA HOSPITAL ROOFS: A CASE STUDY

Andrea Nobili, Ph.D., P.E.[1] and Federico O. Falope, P.E.[2]

ABSTRACT

In this paper, the mechanical performance of concrete beams strengthened by an impregnated Carbon Fabric Reinforced Cementitious Matrix (CFRCM) composite is investigated. The study is aimed at the rehabilitation of the Finale Emilia hospital roofs, severely damaged by the 2012 Northern Italy earthquake. A 8-m-long concrete beam could be taken from the building for reinforcement and testing in a beam test setup. The composite is designed to be externally applied to the existing thin clay tile layer bonded to the concrete beam intrados. Two lamination cycles are considered, which differ in the way the partially-organic adhesion promoter is applied to the fabric. It is found that impregnation thorough fabric immersion provides a 1.5-fold increase in the ultimate strength of the strengthened beam compared to expedited impregnation with a brush. Besides, clay tiles make a very good supporting substrate, to the extent that cohesive fracture at the tile/concrete interface takes place on the verge of concrete failure near the hinge zone. Conversely, expedited impregnation of the carbon fabric with the adhesion promoter is unable to provide adequate fabric/matrix adhesion and leads to delamination failure. Estimates of the adhesion strength, of the optimal bonded length and of the composite as well as of the concrete strain at failure are also provided.

[1]Dipartimento di Ingegneria Enzo Ferrari, Università degli Studi di Modena e Reggio Emilia, via Vignolese 905, 41125 Modena, Italy. (Corresponding author) E-mail:andrea.nobili@unimore.it

[2]Dipartimento di Ingegneria Enzo Ferrari, Università degli Studi di Modena e Reggio Emilia, via Vignolese 905, 41125 Modena, Italy. E-mail:federicooyedeji.falope@unimore.it

INTRODUCTION

Reinforcement and rehabilitation of structurally deficient structures sets a difficult engineering challenge. Historically, jacketing with new concrete bond with surface adhesive or epoxy bonded steel plates have long been the preferred options to retrofit flexural members (Blanksvärd and Täljsten 2008). In more recent times, a number of different technologies have been made available, ranging from glass fiber reinforced polymer (GFRP) composite plates (Saadatmanesh and Ehsani 1991; Rahimi and Hutchinson 2001), carbon fiber reinforced polymer (CFRP) composites (Norris et al. 1997; Mouring et al. 2001), high strength composites (Ombres 2011a; Arboleda 2014). In particular, great attention has been recently drawn towards brittle inorganic cement-based matrix composites, as opposed to ductile polymeric-based ones, in light of some limitations of the organic binder (Bentur and Mindess 2006; Toutanji and Deng 2007). The inorganic matrix may accommodate different kinds of reinforcement, either in the shape of long fibers arranged in sheets or nets (fabric reinforced cementitious matrix, FRCM, or textile reinforced concrete, TRC), such as polyparaphenylene benzobi-soxazole (PBO) (Ombres 2011b), glass or carbon fabric (Babaeidarabad et al. 2014) or randomly dispersed short fibers, such as polypropylene (Lanzoni et al. 2012; Nobili et al. 2013). Besides, reinforcement may be dry, in direct contact with the matrix, or impregnated through some adhesion promoter, which enhances the bond with the binder and hinders slippage.

In this paper, a Carbon Fabric Reinforced Cementitious Matrix (CFRCM) composite is designed and tested for the rehabilitation of the concrete-joist-and-hollow-block roofs of the "Ospedale Civile degli Infermi" (ICC-Evaluation Service 2013). This is a four-building hospital facility located in Finale Emilia, which had been severely damaged by the 2012 Northern Italy earthquake (Tertulliani et al. 2012). The main hospital building (coded H1) is a masonry unit which grew out of the former Santo Spirito church, whose conception dates

2

back to 1668. Although several literature contributions exist dealing with strengthening of reinforced concrete (RC) beams by an externally applied FRCM composite (Triantafillou and Papanicolaou 2005; Brückner et al. 2006; Al-Salloum et al. 2012; Loreto et al. 2013), this paper investigates some novel and distinctive features. First, performance is assessed in a beam test on roof beams taken from a case study application. Second, roof beams had been cast onto a thin layer of clay tiles to provide material continuity with the hollow blocks and an uniform substrate for plaster adhesion. Assessing the composite/tile/concrete bond strength is crucial to developing a reliable reinforcement system directly applied onto the tile surface. Indeed, mechanical removal of the tile layer prior strengthening is extremely costly and time consuming, in light of the large area to be treated and of the extensive damage this would cause to the underlying concrete. Besides, the clay tile provides a rough surface suitable for direct lamination. Third, fabric is impregnated by a partially-organic adhesion promoter and the extent of this impregnation deeply affects performance.

EXPERIMENTAL PROGRAM

Application of the CFRCM composite

A preliminary analysis of the main building found more than ten different types of roofs, for the largest part constituted by concrete beams with hollow blocks in between, with different slab thickness and orientation (Fig.1). A roof typical cross-section is shown in Fig.2. An impregnated CFRCM composite is considered to be bonded at the intrados of the concrete beams taken from the Finale Emilia hospital roof. The composite material is applied according to the following steps:

1. the substrate (i.e. the clay tile) is wetted and then a water-based liquid inorganic adhesion promoter is applied with a brush;

2. a first mortar bed, roughly 5 mm thick, is laid;

3. cut-to-size pairs of uni-directional carbon fabric reinforcement sheets are impregnated by the adhesion promoter through immersion and then squeezed out to eliminate the

3

76 excess of impregnating agent (only for Cycle A, see Fig.3);

77   4. a first sheet of uni-directional carbon fabric reinforcement is placed onto the mortar

78   bed and then rolled to dispense with trapped air bubbles (Fig.4);

79   5. a second sheet of the same uni-directional carbon fabric reinforcement is placed and

80   then rolled;

81   6. a second and final mortar bed, roughly 5 mm thick, is laid on top.

82 Alongside this treatment, which is termed Cycle A, a simpler process is considered, named

83 Cycle B, which dispenses with step 3. According to this simpler application cycle, the liquid

84 impregnation agent is applied with a brush directly to the carbon fabric already placed on

85 the mortar bed, both after steps 4 and 5 (Fig.3). The reason for this second option is that the

86 expected performance decay could be weighted against the advantage of a more expedited

87 process and the lower cost it conveys. All materials adopted in the analysis are commercially

88 available and their main properties are gathered in Table 1 for the mortar and in Table 2

89 for the fabric. The mortar (coded B) and the impregnation agent are characterized as single

90 components in Nobili (2016). The main reason for adopting this fairly low-strength mortar is

91 compatibility with the clay tile mechanical properties. Besides, this mortar, in conjunction

92 with the adopted adhesion promoter, has proved very effective in developing a strong bond

93 with the carbon fabric.

94 **Experimental setup**

95   In order to avoid weakening an already poorly performing structure, only a single 8-m-

96 long beam could be taken from the hospital roof (the original location of this beam is shown

97 in Fig.1). For transportation convenience, the beam was cut into 5 pieces, between 1.2 to

98 1.4 m long. The roof beam is fitted with a variable-along-the-length longitudinal steel bar

99 reinforcement, which roughly follows the bending moment diagram. Rebar surface is not

100 patterned. The mid-span longitudinal reinforcement is given by $3\varnothing16 + 2\varnothing6$ mm and by

101 $1\varnothing16$ mm, respectively for lower and upper section reinforcement (see Fig.5). Conversely, the

4

beam end longitudinal reinforcement features $1\varnothing 6$ mm (lower) and $1\varnothing 12$ mm (upper section). Table 3 gathers the cross-section inertial properties. It should be emphasized that the longitudinal rebar distribution is incompatible with modern seismic design, for no provision is taken against bending moment sign inversion. The beam pieces were further cut into a total of 15 400-mm-long portions, each endowed with a different amount of longitudinal steel rebars according to its location in the original joist. Transverse reinforcement is very weak and only $1\varnothing 6/500$ mm steel bar could be detected through pachometer testing. According to the Italian Building Code (2008, §4.1.2.1.3.2), the theoretical ultimate shear strength amounts to

$$V_{Rcd} = 22.4 \text{ kN}. \tag{1}$$

In view of the high danger of brittle failure due to shear in a plain bending test, a beam test (alias traction-through-bending test) on pairs of beam portions joined together through a steel hinge was adopted (RILEM 1994). The test schematic is presented in Fig.6.

The joist pairs are joined together via removable mechanical connectors and then laminated according to either Cycle A or B. After 28-day curing, they are tested in a four-point bending test arrangement, through a Metro Com Engineering 7170S02 machine. On the overall, 7 joist pairs could be tested, 3 laminated according to Cycle A and 4 to Cycle B. A Q-400 Dantec Dynamics Digital Imaging Correlation (DIC) system was adopted to monitor the displacement field of the beam tests (Becker et al.). The beam concrete properties were determined through crash testing of drilled concrete cores. Indirect measurement through concrete hammer testing (PCE-HT-225A) was also pursued but it provided scattered results around an unrealistically high mean. Finally, a qualitative indication of concrete carbonation was obtained through phenolphthalein titration.

EXPERIMENTAL RESULTS

Beam tests

Seven joist pairs, labeled from A1 to A7, were tested in a beam test through a four-point-bending machine equipped with a 200 kN load cell. No provision was taken against shear failure on the grounds that laminate debonding was expected to take place prior to shear failure (the latter taking place much before bending failure). According to CNR DT200 2004, §4.1.1, the optimal bonded length, l_e, beyond which no increase of the load transferred by the composite may be obtained, can be estimated as

$$l_e = \max \left(\frac{1}{\gamma_{Rd} f_{bd}} \sqrt{\frac{\pi^2 E_f t_f \Gamma_{fd}}{2}}, 200 \text{ mm} \right) = 245 \text{ mm} \qquad (2)$$

where Γ_{fd} is the specific fracture energy which depends on the ultimate slip s_u (see also D'Ambrisi et al. 2013 for a suitable choice of s_u for FRCM materials) and parameters are given in Table 4. Clearly, for maximum performance, the bonded length l_b should exceed l_e. Indeed, a bonded length $l_b = 300$ mm was considered with no special anchoring device (e.g. U-wrapped fabric, transverse bars, abrasive blasting of the substrate surface etc.). The bending test was carried out under displacement control at 1 mm/min knife speed. Fig.7 gathers the results of the beam test while Fig.8 presents the failure mechanism for each specimen. Failure in specimens A1–A3, treated according to Cycle A, is either due to cohesive fracture in the thin tile layer, also known as intermediate debonding, or to tensile failure in the concrete (for a brief description of the different fracture mechanisms see CNR DT200 (2004)). Indeed, specimen A2 displayed clear evidence of tensile failure in the concrete near the hinge, which was accompanied by mixed cohesive fracture at the laminate interface.

Conversely, delamination of the fabric with fracture taking place at the fabric/matrix interface is always met in specimens A4–A7, prepared according to Cycle B. The difference in the failure mechanism reflects itself in a sharp difference among the ultimate loads, which exceed 60 kN for Cycle A as opposed to well below 50 kN for Cycle B. It is observed that

6

ultimate loads within Cycle A were remarkably consistent (cfr. error bar in Fig.10).

Image Correlation results

A Q400 Dantec Dynamics Digital Image Correlation system was employed to acquire the displacement field along the beam test through application to the specimen side of a fine coarse speckle array. A preliminary zero-displacement data acquisition allowed assessing a 20 μm displacement background noise level (resolution). A technical problem prevented recording displacement data of the A6 specimen. Two reference lines, named L and R for the left and right element, respectively, are drawn symmetrically about the hinge. The deformation of such lines (i.e. longitudinal displacement with respect to the original position) is displayed in Fig.9 for specimen A2 at 60% of the ultimate load and just prior to failure. The symmetry of the left-right line displacement is remarkable and holds for all specimens.

Compression test of concrete cores

After bending, four concrete cores were drilled in the joist longitudinal direction out of two joist pairs. Owing to the cross-sectional shape, cores were 50 mm in diameter and about 100 mm in height. After drilling, core specimens were regularized. Uni-axial compression tests were performed through a Metro Com Engineering E7072C300 machine, equipped with a 3000 kN load cell, under force control, at a loading rate of 0.5 MPa/s. Compressive strength results are recorded in Table 5, together with their adjusted value, according to Kim and Eo (1990) and Benjamin and Cornell (1970), to compensate for the non-standard specimen size. Maximum aggregate size is about 15 mm. On the overall, results showed good consistency, with a relative standard deviation (alias coefficient of variation, CV) of about 12%. A longitudinal crack pattern consistently developed at failure, which agrees well with an uni-axial compression failure mode (Neville and Brooks 1987). Indirect concrete hammer testing produced scattered and unrealistically over-estimated results. Finally, phenolphthalein titration provided little evidence of carbonation, as expected for a indoor structural element.

DISCUSSION

Theoretical flexural strength

The ultimate theoretical flexural strength of the unreinforced cross-section at mid-span is, in the stress block approximation (Italian Building Code 2008, §4.1.2.1.2), $M_{Rd,\mathrm{midspan}} = 32.2$ kNm which, compared with the shear strength (1), shows that a plain bending test would have been possible for a very long specimen, such that $l_A \geq 2.87$ m$+l_F$. A similar calculation shows that the beam end section unreinforced strength amounts to $M_{Rd,\mathrm{ends}} = 20.5$ kNm and, in a doubly built-in configuration, flexural failure still occurs at midspan. In this respect, the existing longitudinal reinforcement provides adequate flexural strength and the composite adds a comparatively small contribution to it. However, when considering bending moment sign inversion, the beam end section appears exceedingly weak at the intrados, with an ultimate theoretical strength of the unreinforced section of 12.6 kNm. Application of the composite reinforcement leads to a theoretical strength of 21.9 kNm for the end section, which warrants almost uniform flexural resistance for the beam in the case of bending moment sign inversion.

Adhesion and laminate strength

The beam test setup easily lead to the evaluation of the ultimate load for the composite as

$$N_u = \frac{M_u}{d}, \tag{3}$$

where $M_u = P(l_A - l_F)/4$ is the ultimate bending moment (Fig.6), $d = 210$ mm the lever arm and N_u the ultimate normal force conveyed through the hinge and the laminate. Once the normal force N_u is determined, the ultimate average shear stress easily follows

$$\tau_{av} = \frac{N_u}{A_b}, \tag{4}$$

where $A_b = b_4 l_b = 39000$ mm^2 is the bonded area and l_b the bonded length.

The computed average shear stress, τ_{av}, for the specimens treated according to Cycle A is compatible with a clay tile failure mechanism and it is an important parameter to

8

design the roof reinforcement. Besides, evaluating the steel hinge net contact area with the cross-section, $A_h = 8450$ mm^2, the average compressive stress $\sigma = N/A_h \approx -4.09$ MPa and the corresponding tensile stress (through Mohr's circle) $\sigma/2 \approx 2.04$ MPa, are easily determined. In particular, the tensile stress far exceeds the ultimate tensile strength of concrete $f_{ctm} \sim 0.46$ MPa, as evaluated according to Italian Building Code (2008, §11.2.10.2), which fact may help explain heavy concrete damage incurred at failure for specimens A1, A3 and especially A2. Delamination at the fabric/matrix interface appears to be determined by ineffective impregnation of the fabric reinforcement by the adhesion promoter in Cycle B. In fact, all specimens treated according to Cycle B fail to provide consistent levels of ultimate strength in the beam test.

Deformation at failure

The digitally acquired displacement field provides a discrete approximation of the strain field both in the concrete and, with lower accuracy, in the composite. The mean concrete compressive strain at failure (near the hinge) for specimens A1–A3 is 1.24‰ with $CV = 0.25$‰, while the corresponding (tensile) mean strain in the composite is 1.04% with $CV = 0.75\%$. It is interesting to observe that, introducing the concrete mean compressive strain as the limiting deformation at failure in a stress block model, the theoretical strength of the cross-section in a beam test, i.e. omitting the lower section rebars and assuming perfect composite/substrate adhesion, amounts to 8.7 kNm (almost irrespectively whether it is mid-span or end section), which is 16% greater than the average ultimate bending moment, M_u, as measured for specimens A1–A3 (see Table 6). However, the corresponding ultimate force in the composite is 34.5 kNm, which differ very little (+1.4%) from the mean experimental value. Finally, we note that the tensile mean strain in the composite at failure is very close to the composite ultimate strain, ϵ_{fu}, which, according to ICC-Evaluation Service (2013), is 0.94% with $CV = 0.19\%$.

CONCLUSIONS

In this paper, the mechanical performance of an impregnated Carbon Fabric Reinforced

9

Cementitious Matrix (CFRCM) composite is considered. The composite is intended to strengthen the RC roof beams of the Finale Emilia hospital, severely damaged by the 2012 Northern Italy earthquake. The following conclusions can be drawn from the foregoing analysis:

- A beam test, in the absence of anchoring devices, was found effective in assessing the composite strength, despite the variability of the longitudinal and the deficiency of the traversal steel bar reinforcement and despite the surprisingly poor mechanical performance of the concrete.

- External application of the composite to the thin clay tile layer onto which beams had been originally cast is safe and economic: cohesive fracture at the tile/concrete interface takes place at failure on the verge of brittle compressive failure in the concrete.

- Deformation data obtained from Digital Image Correlation give a tensile mean strain in the composite at failure around 1.04%, which is very close to the design strain, while the mean compressive strain in the concrete (near the hinge) is $1.24\%_0$, which is lower than expected (given that delamination occurs on the verge of concrete failure).

- Impregnation of the fabric needs be carefully considered. Indeed, impregnation through immersion provides a 1.5-fold increase of the ultimate strength with respect to expedited impregnation. Furthermore, lack of adhesion due to insufficient impregnation consistently leads to fabric slippage in the matrix and, finally, debonding.

- Estimates of the composite strength, of the average shear strength at the composite/tile interface and of the optimal bonded length are given.

- Although the existing beam longitudinal steel bar reinforcement is adequate in a static analysis, composite strengthening at the intrados is required when considering seismic design and the possibility of bending moment sign inversion.

ACKNOWLEDGMENTS

10

REFERENCES

259 Al-Salloum, Y. A., Elsanadedy, H. M., Alsayed, S. H., and Iqbal, R. A. (2012). "Experimental
260 and numerical study for the shear strengthening of reinforced concrete beams using textile-
261 reinforced mortar." *Journal of Composites for Construction*, 16(1), 74–90.

262 Arboleda, D. (2014). "Fabric reinforced cementitious matrix (FRCM) composites for in-
263 frastructure strengthening and rehabilitation: Characterization methods." Ph.D. thesis,
264 University of Miami, University of Miami. Open Access Dissertation. Paper 1282.

265 Babaeidarabad, S., Loreto, G., and Nanni, A. (2014). "Flexural strengthening of RC beams
266 with an externally bonded fabric-reinforced cementitious matrix." *Journal of Composites
267 for Construction*, 18(5), 04014009.

268 Becker, T., Splitthof, K., Siebert, T., and Kletting, P. *Digital 3D-Correlation System Q-400.*
269 Dantec Dynamics. http://www.dantecdynamics.com.

270 Benjamin, J. and Cornell, C. (1970). *Probability, Statistics, and Decision for Civil Engineers.*
271 McGraw-Hill Publishing Company.

272 Bentur, A. and Mindess, S. (2006). *Fibre reinforced cementitious composites.* CRC Press.

273 Blanksvärd, T. and Täljsten, B. (2008). "Strengthening of concrete structures with cement
274 based bonded composites." *Journal of Nordic Concrete Research*, 38, 133–153.

275 Brückner, A., Ortlepp, R., and Curbach, M. (2006). "Textile reinforced concrete for strength-
276 ening in bending and shear." *Materials and structures*, 39(8), 741–748.

277 CNR DT200 (2004). "Guide for the design and construction of an externally bonded FRP
278 system for strengthening existing structures." *Italian National Research Council, Rome*
279 R1/2013.

280 D'Ambrisi, A., Feo, L., and Focacci, F. (2013). "Experimental and analytical investigation

11

on bond between carbon-frcm materials and masonry." *Composites Part B: Engineering*, 46, 15–20.

ICC-Evaluation Service (2013). "Acceptance criteria for masonry and concrete strengthening using fiber-reinforced cementitious matrix (FRCM) composite systems." *AC434*.

Italian Building Code (2008). "DM 14.01.2008: Norme tecniche per le costruzioni." *Rome: Italian Ministry of Infrastructures and Transportation*.

Kim, J. K. and Eo, S. (1990). "Size effect in concrete specimens with dissimilar initial cracks." *Magazine of Concrete Research*, 42(153), 233–238.

Lanzoni, L., Nobili, A., and Tarantino, A. (2012). "Performance evaluation of a polypropylene-based draw-wired fibre for concrete structures." *Construction and Building Materials*, 28(1), 798–806.

Loreto, G., Leardini, L., Arboleda, D., and Nanni, A. (2013). "Performance of RC slab-type elements strengthened with fabric-reinforced cementitious-matrix composites." *Journal of Composites for Construction*, 18(3), A4013003.

Mouring, S. E., Barton, O., and Simmons, D. (2001). "Reinforced concrete beams externally retrofitted with advanced composites." *Advanced Composite Materials*, 10(2-3), 139–146.

Neville, A. M. and Brooks, J. J. (1987). *Concrete technology.* Longman Scientific & Technical.

Nobili, A. (2016). "Durability assessment of impregnated glass fabric reinforced cementitious matrix (GFRCM) composites in the alkaline and saline environments." *Construction and Building Materials*, 105, 465–471.

Nobili, A., Lanzoni, L., and Tarantino, A. (2013). "Experimental investigation and monitoring of a polypropylene-based fiber reinforced concrete road pavement." *Construction and Building Materials*, 47, 888–895.

Norris, T., Saadatmanesh, H., and Ehsani, M. R. (1997). "Shear and flexural strengthening of RC beams with carbon fiber sheets." *Journal of structural engineering*, 123(7), 903–911.

Ombres, L. (2011a). "Flexural analysis of reinforced concrete beams strengthened with a cement based high strength composite material." *Composite Structures*, 94(1), 143–155.

12

Ombres, L. (2011b). "Structural performances of PBO FRCM-strengthened RC beams." *Proceedings of the ICE-Structures and Buildings*, 164(4), 265–272.

Rahimi, H. and Hutchinson, A. (2001). "Concrete beams strengthened with externally bonded FRP plates." *Journal of composites for construction*, 5(1), 44–56.

RILEM, T. (1994). "RC 5 Bond test for reinforcement steel. 1. Beam test, 1982." *RILEM Recommendations for the Testing and Use of Constructions Materials*, 213–217.

Saadatmanesh, H. and Ehsani, M. R. (1991). "RC beams strengthened with GFRP plates. I: Experimental study." *Journal of Structural Engineering*, 117(11), 3417–3433.

Tertulliani, A., Arcoraci, L., Berardi, M., Bernardini, F., Brizuela, B., Castellano, C., Del Mese, S., Ercolani, E., Graziani, L., Maramai, A., et al. (2012). "The Emilia 2012 sequence: a macroseismic survey." *Annals of Geophysics*, 55(4).

Toutanji, H. and Deng, Y. (2007). "Comparison between organic and inorganic matrices for RC beams strengthened with carbon fiber sheets." *Journal of Composites for Construction*, 11(5), 507–513.

Triantafillou, T. C. and Papanicolaou, C. G. (2005). "Textile reinforced mortars (TRM) versus fiber reinforced polymers (FRP) as strengthening materials of concrete structures." *Proceedings of the 7th ACI International Symposium on Fibre-Reinforced (FRP) Polymer Reinforcement for Concrete Structures*, American Concrete Institute, 99–118.

List of Tables

14

Characteristic	Unit	Value
Mean compression strength after 28 days	MPa	6.5
Mean flexural strength after 28 days	MPa	3
Support adhesion strength after 28 day	MPa	1
Water content	%	23
Aggregate maximum size	mm	0.7
Longitudinal elastic modulus	GPa	11
Water vapor permeability, μ	-	12

TABLE 1. Mortars properties

Characteristic	Unit	Value
Density	g/cm^2	160
Elastic modulus, E_f	GPa	210
Ultimate strength, f_{uf}	GPa	≥ 2.0
Ultimate strain, ϵ_{uf}	%	≥ 2.1
Cross-section area/unit width	mm^2/cm	0.88

TABLE 2. Fabric properties in the principal direction

Inertial property	Unit	Value
Area, A	mm^2	19500
Center of mass, x_G	mm	0
Center of mass, y_G	mm	119
Principal moment of inertia, I_{x_G}	mm^4	12391
Principal moment of inertia, I_{y_G}	mm^4	1358

TABLE 3. Cross-section inertial properties

Parameter	Unit	Value
γ_{rd}	-	1.25
k_b	-	1
k_G	-	0.037
FC	-	1.2
Γ_{fk}	N mm^{-2}	0.118
f_{bd}	N mm^{-3}	2.36
s_u	mm	0.1

TABLE 4. Parameters for the evaluation of the optimal bonded length l_e

Core	Cylinder strength [MPa]		
	Raw	Adjusted	
		(Kim and Eo 1990)	(Benjamin and Cornell 1970)
C1	9.89	10.78	10.81
C2	8.48	9.34	9.26
C3	8.00	8.75	8.75
C4	10.36	11.28	11.32
mean	9.18	10.03	10.03
std. dev.	1.12	1.18	1.22
rel.std. dev. [%]	12.20	11.83	12.20

TABLE 5. Compression results

Specimen	FM	Cycle	M_u [kNm]	N_u [kN]	τ_{av} [MPa]	τ_{av} mean [MPa]	Std.dev [MPa]
A1	c	A	7.11	33.88	0.86		
A2	c+t	A	7.25	34.56	0.88	0.88	0.02
A3	c	A	7.4	35.25	0.90		
A4	d	B	5.4	25.74	0.66		
A5	d	B	4.02	19.16	0.49	0.57	0.08
A6	d	B	4.27	20.35	0.52		
A7	d	B	5.09	24.26	0.62		

TABLE 6. Beam test results; FM=Failure mechanism: (c) cohesive in the brick layer, (t) traction in the concrete, (d) delamination at the fabric/matrix interface

List of Figures

Test concrete
beam location

FIG. 1. Roof system at ground floor for the hospital main building (H1)
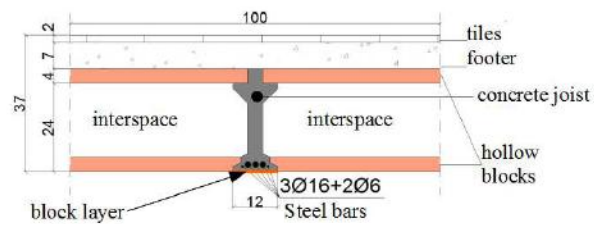
FIG. 2. Roof typical cross-section (dimensions in mm)
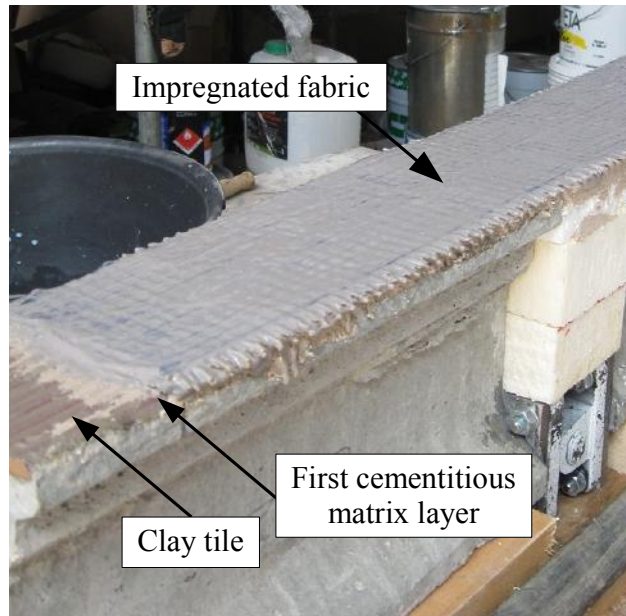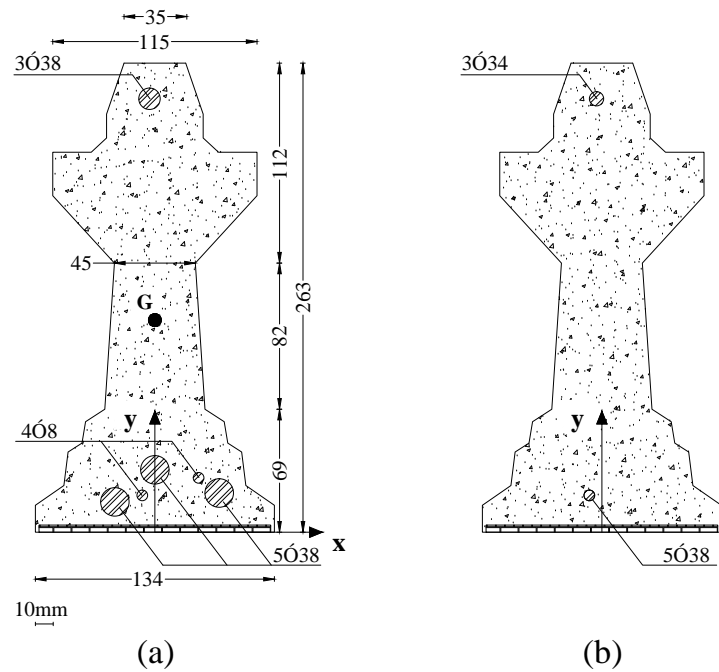
<div align="center">(a)   (b)</div>

FIG. 3. Application of the liquid impregnation agent to the cut-to-size carbon fabric: (a) impregnation through immersion (Cycle A), (b) application with a brush to the carbon fabric already placed on the mortar bed (Cycle B)
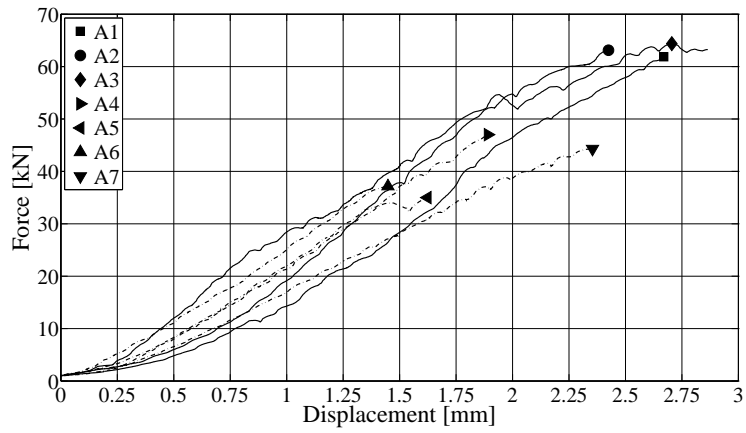
FIG. 4. The roof concrete beam is placed upside down for lamination (clay tile on top, steel hinge for the beam test at the bottom)

FIG. 5. Concrete beam mid-span (a) and beam end (b) cross-sections (clay tile at the bottom) and reference system
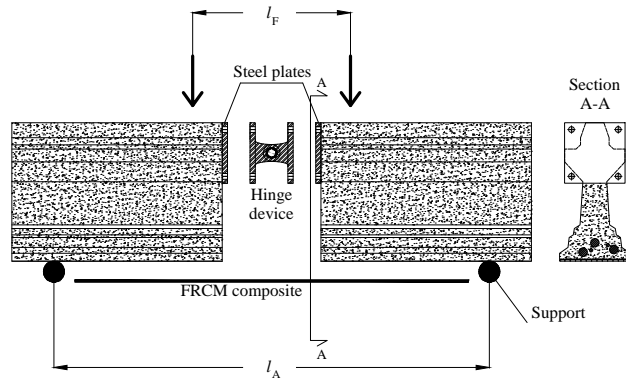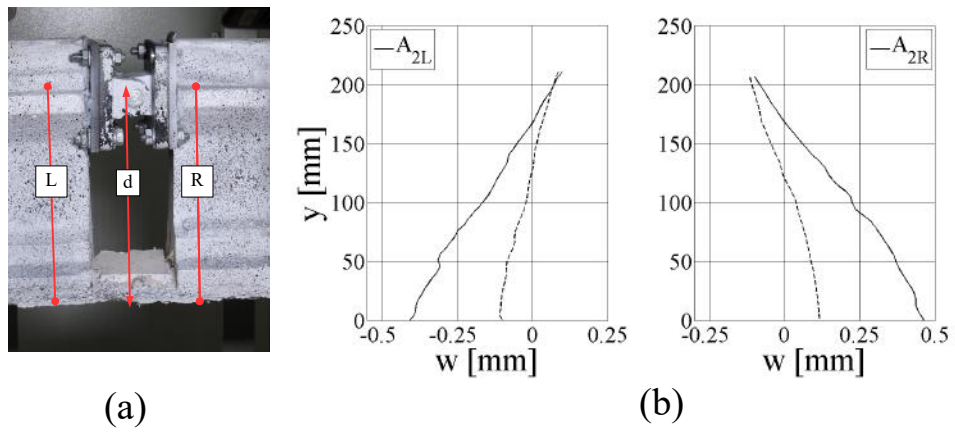
**FIG. 6. Schematic of a beam test:** $l_F = 300$ **mm,** $l_A = 900$ **mm**

FIG. 7. Beam test results - solid curves belong to Cycle A, dashed curves to Cycle B

FIG. 8. Failure modes: cohesive fracture (specimen A1 and A3), tensile failure in the concrete (A2), delamination (A4,A5,A7)

(a)   (b)

FIG. 9. Location of the reference lines L and R (a) and their axial displacement w vs. cross-sectional height y at 100% (solid) and at 60% (dashed) of the ultimate load for specimen A2 (b). Reference system as in Fig.5

30
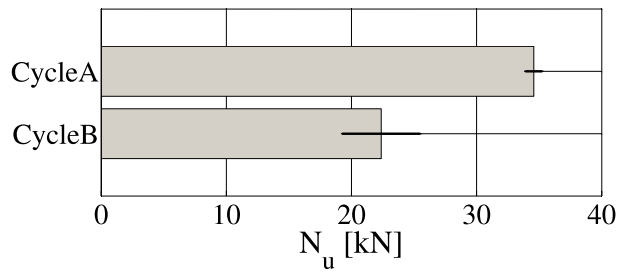
FIG. 10. Ultimate load N and one-standard deviation bar